Int. J. Multiphase Flow Vol. 16, No. 5, pp. 751–759, 1990
Printed in Great Britain.

0301-9322/90 $3.00 + 0.00

EVALUATION OF A NUMERICAL CRITICAL PIPE FLOW MODEL WITH WALL NUCLEATION

B. C. R. EWAN[1] and K. MOODIE[2]

[1]Department of Mechanical and Process Engineering, University of Sheffield, Sheffield, England

[2]Explosion & Flame Laboratory, Health & Safety Executive, Buxton, England

(*Received* 1 *August* 1988; *in revised form* 25 *February* 1990)

Abstract—Results are reported of the application of an existing two-phase critical pipe flow solution procedure based on numerical integration of the conservation equations for each phase. Modifications have been made which incorporate wall nucleation, as observed experimentally, and results are compared with a wide range of reported and tested cases.

Key Words: critical flow, superheated releases, pipe flow

INTRODUCTION

In most cases of release from chemical reactors at high temperature and pressure or from pressurized hydrocarbons, the flow at the control section is critical and this may be an expansion within the release path or an exit point to atmosphere. In this situation the release parameters are dependent only on the source conditions and geometry. In recent years the increasing safety analysis applied to chemical plant and bulk transport systems has widened the scope of critical flow treatments, and there is a desire that these be routinely available to safety authorities.

Several models are available to describe the problem and these include analytical types, which embody a number of simplifying assumptions concerning equilibrium, relative phase motion etc., as well as those which solve the conservation equations numerically for each phase and include inter-phase coupling terms.

A review of the literature confirms the general view that the analytical models are best suited to release paths which are sufficiently long to enable some degree of inter-phase mass transfer and equilibration. It is recognized however that in many loss situations, the release path may be only a few centimetres, and it may then be necessary to interpolate mass flow rates between liquid jet and two-phase equilibrium regimes.

Alternative solution procedures of a more fundamental nature have become available in recent years and are exemplified in the work of Ardron (1978) and Richter (1983). Both of these authors approach the problem by a stepwise integration of the conservation equations for each phase along the release path. This approach is particularly attractive since it greatly simplifies the incorporation and modification of such terms as liquid–vapour interaction, vapour source, liquid–wall friction and heat transfer.

Ardron (1978) considered the vapour phase to consist of bubbles, and developed a bubble generation model based on homogeneous and heterogeneous nucleation. Richter (1983), on the other hand, initiated the evaporation process using an initial fixed bubble population, but recognized that as the void fraction grew, bubble coalescence should take place giving rise to flow regimes with different interaction and heat transfer characteristics.

A recent review of the performance of several codes, both analytical and numerical, by Levy Inc. (1982) against the data from the Marviken tests, has concluded that the approach due to Richter provided the overall best results. The present work builds on the work of this author by incorporating observed experimental features into the bubble generation scheme, whilst retaining the feature of different flow regimes depending on void fraction.

A range of release experiments with R11 are also described and model predictions are compared with these as well as a number of literature cases.

DESCRIPTION OF THE RELEASE PROCESS

Much of the effort in studying critical releases has been devoted to a simple straight pipe release geometry. A common assumption in many analytical models is that an entrance void fraction exists, either due to impurity bubbles or a homogeneous nucleation process. Figure 1 shows a photograph of a critical flow of R11 inside a rectangular flow cell. This cell consists of two opposed glass walls and two opposed metal walls with machined surfaces. The inner channel is a smoothly contoured funnel from 50 × 4 mm at the source tank to 7 × 4 mm in the straight channel, this being 120 mm long. The cases shown are typical of all tests carried out using both machined metal and polycarbonate walls and show that the dominant source of nucleation bubbles is the metal wall area with no bubbles appearing to arise around the glass surface or within the body of the channel.

It seems likely therefore that nucleation on the wall is responsible for bubble creation and this is likely to be so for most cases of interest where liquid impurity levels are not excessive. A general description of the release process can thus be given with reference to figure 2.

Liquid accelerates into the pipe and experiences a pressure head loss. For initially saturated liquids, this head loss creates a superheated state and nucleation bubbles form at the walls, due to a pre-existing population of wall cavities. The driving force for bubble creation and subsequent growth is therefore the excessive temperature of the liquid above the saturation curve corresponding to the local pressure. Evaporation is taken to occur at the liquid bubble interface and wall nucleation can continue along the pipe length.

Further continuous pressure losses arise due to liquid wall friction and more importantly due to the evaporation process. As a result, the degree of superheat tends to increase and consequently the evaporation rate. In addition, the expanding bubbles begin to interact and coalesce and adopt different heat and mass transfer modes. In many flows, the evaporation proceeds to the point where the liquid is forced to the pipe walls and the gas occupies a rapidly moving core. In critical flows, the acceleration has progressed to the point where the flow is choked, and this is characterized by very steep pressure gradients located at the control section, where the pressure is above ambient.

Figure 3 shows typical spray patterns at a pipe exit with R11 releases. In the higher pressure and higher superheat case, the exit behaviour is markedly different due to the different values associated with exit pressure, void fraction and temperature, and it is the objective of all predictive procedures to ultimately account for these to enable a better link with subsequent spray behaviour.

NUMERICAL INTEGRATION SOLUTION PROCEDURE

Due account has been taken of the above observations in the solution procedure described below. The calculation method employed is based on the approach of Richter (1983) and uses a stepwise numerical integration procedure along the length of the pipe together with the differential equations of mass, momentum and energy conservation. This has been fully described by Richter, and is repeated here briefly along with the changes which have been implemented to represent the nucleation process.

The conservation equations are written for each phase separately and include liquid–vapour interaction terms. In this way relative phase velocities evolve naturally through the definition of the interaction forces.

Conservation of mass

For the liquid,

$$\frac{1}{W_L}\frac{dW_L}{dZ} = \frac{1}{\rho_L}\frac{d\rho_L}{dZ} + \frac{1}{V_L}\frac{dV_L}{dZ} - \frac{1}{1-\epsilon}\frac{d\epsilon}{dZ} + \frac{1}{A}\frac{dA}{dZ}. \quad [1]$$

For the vapour,

$$\frac{1}{W_G}\frac{dW_G}{dZ} = \frac{1}{\rho_G}\frac{d\rho_G}{dZ} + \frac{1}{V_G}\frac{dV_G}{dZ} + \frac{1}{\epsilon}\frac{d\epsilon}{dZ} + \frac{1}{A}\frac{dA}{dZ}. \quad [2]$$

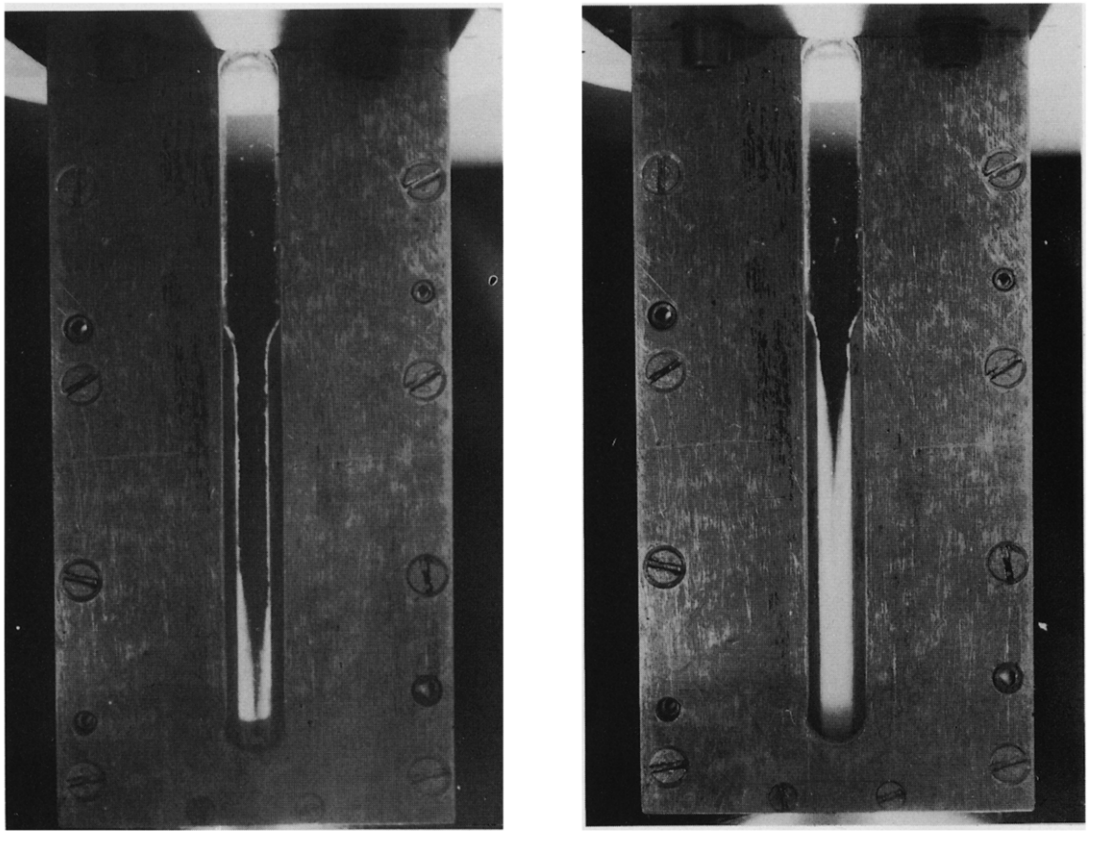

(a) (b)

Figure 1. Examples of nucleating bubble patterns in a rectangular flow cell with metal side walls using freon-11: (a) source pressure 0.3 MPa; (b) source pressure 0.7 MPa.

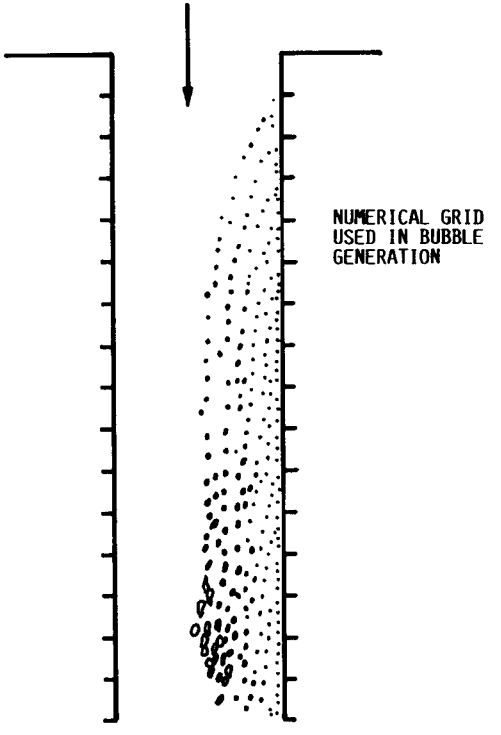

Figure 2. Schematic of superheated liquid flow along the release path showing progressive bubble growth from the side walls, and the cells used in the numerical simulation.

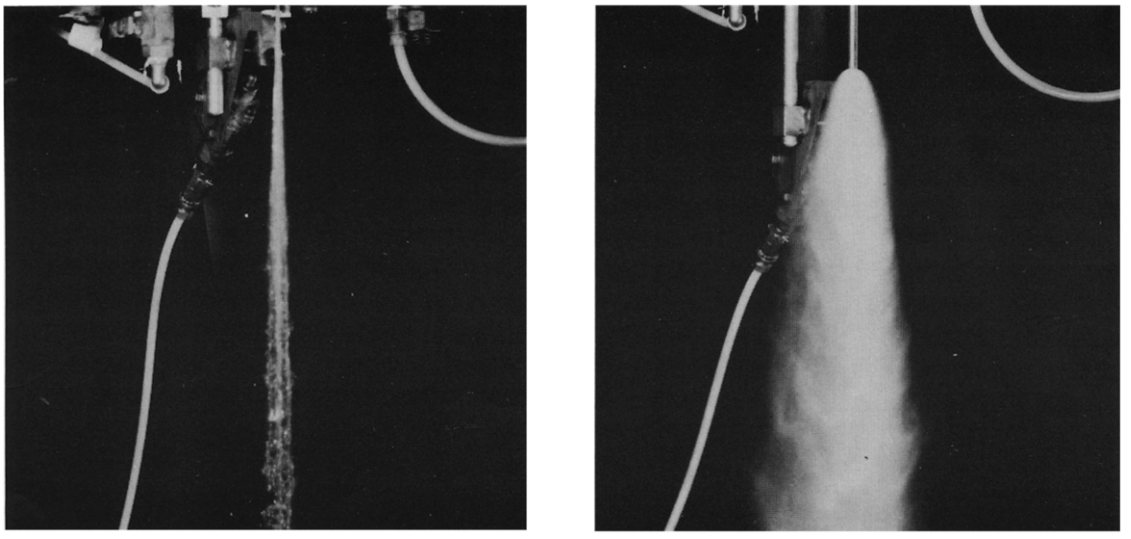

(a) (b)

Figure 3. Different spray patterns at a pipe exit depending on the source pressure with freon-11: (a) source pressure 0.25 MPa; (b) source pressure 0.6 MPa.

Conservation of momentum

For the liquid,

$$\rho_L V_L (1-\epsilon) A \frac{dV_L}{dZ} = -\frac{dP}{dZ}(1-\epsilon) A + F_{LG} A - F_{WL} A - (1-\xi)(V_G - V_L) W \frac{dX}{dZ} - \rho_L g (1-\epsilon) A \cos\theta. \quad [3]$$

For the vapour,

$$\rho_G V_G A \frac{dV_G}{dZ} = -\frac{dP}{dZ}\epsilon A - F_{LG} A - F_{WG} A - \xi(W_G - V_L) W \frac{dX}{dZ} - \rho_G g A \cos\theta. \quad [4]$$

Conservation of energy

$$\frac{dX}{dZ} W\left[(h_G - h_L) + \frac{(V_G^2 - V_L^2)}{2}\right] + W\left(\frac{dh_G}{dZ} + V_G \frac{dV_G}{dZ}\right) + W_L\left(\frac{dh_L}{dZ} + V_L \frac{dV_L}{dZ}\right) + W_G \cos\theta. \quad [5]$$

The evaporation rate is taken to be governed by the heat transfer rate to the liquid–vapour interface and is given, in general, as

$$h_T a_v (T_L - T_G)\epsilon A = \frac{dW_G}{dZ} h_{LG} + W_G \frac{dh_G}{dZ}. \quad [6]$$

In the above we have used the following notation: W—mass flow rate; Z—distance along the pipe; ρ—density; V—velocity; ϵ—void fraction; A—pipe cross-sectional area; F—friction force; P—pressure; ξ—momentum partioning coefficient; g—acceleration due to gravity; θ—discharge angle from the vertical; X—vapour mass fraction; h—specific enthalpy; h_T—heat transfer coefficient; a_v—surface area of bubbles per unit volume of pipe; T—temperature; h_{LG}—latent heat of evaporation; and subscripts L and G represent liquid and vapour, respectively.

The correlations for the liquid–vapour friction F_{LG}, heat transfer coefficient h_T and liquid–wall friction F_{WL}, are taken to be dependent on the flow regime within the pipe, which is designated as bubble flow ($\epsilon < 0.3$), churn turbulent ($0.3 < \epsilon < 0.8$) and annular ($\epsilon > 0.8$). The correlations for each of these regimes have been given in detail in Richter's (1983) work. The liquid–wall friction is evaluated using Churchill's (1977) equation and combined with a two-phase multiplier defined by Martinelli & Nelson (1948). In the initial Richter scheme an entrance population of bubbles was defined with suitable diameter and number density, these being optimized by means of a single

test case. The equations of motion and vapour generation are thus started with initial values of ϵ and W_G.

For the alternative which is proposed in this work, the bubble population is generated by wall nucleation, and for this purpose the pipe length is divided into 16 sections. Bubbles are generated within each section according to the local conditions of site density, superheat and liquid velocity. At any length section n, there are thus $n-1$ bubble populations, growing according to the local heat transfer properties and also the nth developing population which is nucleating and growing within section n. Whilst [6] represents the vapour generation process for a monosize bubble population with the same starting point, it is necessary to redefine these equations for our new scheme, which includes source terms both for bubble growth from within each of the bubble populations from earlier pipe sections, and also from newly nucleated bubbles at the current pipe section.

The gradient for the vapour mass flow rate now becomes

$$\frac{dW_G}{dZ} = \left[\frac{dW_G}{dZ}\right]_{nuc} + \sum_{i=1}^{n}\left[\frac{dW_{Gi}}{dZ}\right]_{ex}, \qquad [7]$$

where the nuc subscript refers to contributions from the nucleation process and ex refers to normal bubble expansion within the bulk liquid. For the proposed scheme of nucleation

$$\left[\frac{dW_G}{dZ}\right]_{nuc} = \Delta N_i \frac{\pi d_0^3}{6} \rho_G A \left[\frac{V_L}{\Delta Z}\right] \qquad [8]$$

and ΔN_i is the change in number density due to nucleation from incremental length ΔZ of the pipe wall.

Equation [9] represents the vapour generation process. In the solution procedure within section n, this is represented by n equations corresponding to each bubble population, which contribute to the total vapour mass change:

$$h_{Ti} a_{vi} (T_L - T_G) \epsilon_i A = \left[\frac{dW_{Gi}}{dZ}\right]_{ex} h_{LG} + W_{Gi}\left[\frac{dh_G}{dZ}\right]. \qquad [9]$$

This means of representing the different bubble populations is also applied to the liquid–vapour friction which is influenced by the bubble diameter and void fraction of the nth population. For pipe regions in which $\epsilon > 0.3$, the bubble nucleation process is still permitted to continue. In these, however, the mass is added to the existing vapour mass and loses its bubble identity.

In order to parameterize the wall nucleation variables, values must be established for d_0, the nucleation bubble diameter, and ΔN_i. This latter is related to the site density parameter ρ_{nuc}, which is the number of sites per unit area of pipe wall, and frequency of generation f_{nuc}:

$$\Delta N_i = \rho_{nuc} f_{nuc} \left[\frac{\Delta Z}{V_L}\right] \frac{4}{D}. \qquad [10]$$

A considerable body of literature data exists on nucleate boiling from heated surfaces (e.g. Lorenz *et al.* 1975) and some indication of the cavity site density and size can be obtained from these. In addition, there are several microscopic studies of nucleation surfaces which indicate the dependence on surface preparation, e.g. Clark *et al.* (1959).

Many of those which involve photographic observation of bubble nucleation are concerned only with natural convection boiling. In these cases only buoyancy forces are involved in the detachment and the larger sites and bubbles are involved. In our case, bubbles are detached by convective forces and are expected to be much smaller and with a greater frequency of detachment. For the present study therefore, attention has been turned to the work of Eddington & Kenning (1979), who have examined nucleation cavity densities from the small-scale sites. In that study of ordinary machined metal surfaces, active cavities have been found to range from 2 to 6 μm with densities in the range 10–250/cm^2. Following from these observations, fixed values have been chosen for ρ_{nuc} and d_0, based on this study, these being

$$\rho_{nuc} = 10^6/\text{m}^2 \quad \text{and} \quad d_0 = 2\,\mu\text{m}.$$

A further indication that such small source bubbles are likely to be present comes from a microscopic study of bubbles within the flow channel which was carried out photographically. Within a few millimetres of the wall, this showed bubble sizes down to 10 μm, which was the resolution limit of the experiment. The frequency of bubble generation must be estimated from available photographic records and analyses. For natural convection nucleate boiling, generation frequencies in the 20 Hz–10 kHz range have been predicted depending on bubble size (Hsu 1965).

Available data on frequency of generation for forced convection is very limited. The photographic study of Berenson & Stone (1965) gives some useful insight in this regard. This concerns R11 flowing at around 1 m/s, and shows bubbles at an active site with a generation frequency of around 3 kHz. It is expected that this higher value is more representative for the small bubbles detaching under our conditions of interest, and this fixed value has been chosen for all cases. However, it is considered necessary to include a dependence of the generation frequency on the degree of superheat at a particular location and on the local liquid velocity. This is due to the fact that the cavity bubble growth rate will be influenced by similar parameters to bubbles within the liquid. Ardron (1978) has indicated that convective heat transfer terms dominate the heat transfer coefficient for free bubbles, and reference to the original correlation used by Richter (1983) for heat transfer coefficient shows this to have a $V_L^{0.5}$ dependence. Rather than attempt to develop a rigorous model for bubble growth and detachment, it is considered more consistent with the one-dimensional nature of the solution procedure to incorporate the main dependent variables and rely on a single case normalization procedure to define the constants. In conclusion therefore f_{nuc} has been chosen to be

$$f_{nuc} = 3000\left[\frac{V_L}{C_V}\right]^{1/2}\frac{(T_L - T_G)}{C_T},$$

where C_T and C_V are normalizing constants. These constants have been chosen with reference to a single test case, which was one of the R11 releases of the present study in which $L = 120$ mm, $d = 4$ mm, $P_0 = 0.4$ MPa and $T_0 = 68°C$. From this, $C_V = 6$ m/s and $C_T = 1.5°C$.

EXPERIMENTAL RELEASE GEOMETRY

The apparatus used for R11 release experiments is shown in figure 4 and consisted of a 30 l. cylindrical vessel with a central piston which could seal an orifice on the lower face. Interchangeable

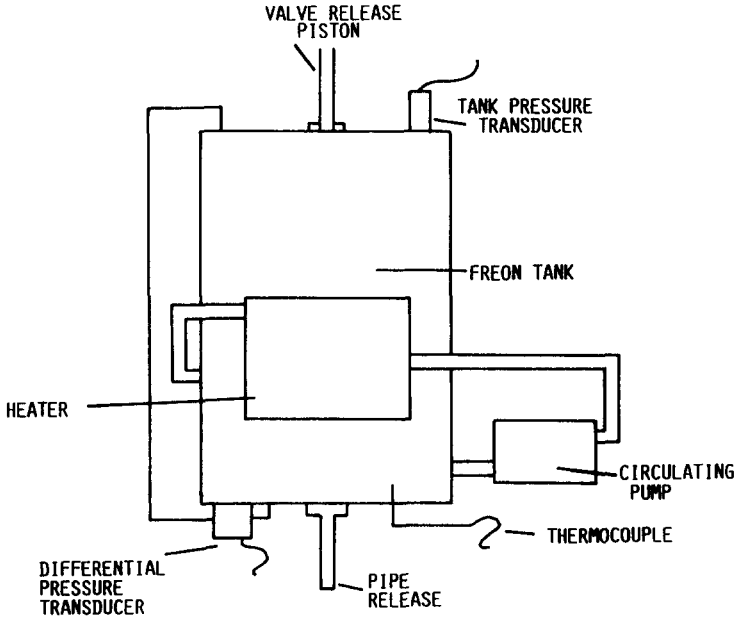

Figure 4. Schematic of the heated tank and the release geometry for the present freon-11 release experiments.

pipe outlets could be fitted to the lower face of the tank. A high-pressure pump circulated the contents around a short external loop which incorporated a 6 kW heating chamber. The tank was instrumented to record vapour pressure above the liquid and liquid temperature by thermocouple. Mass flow rates were determined by monitoring the head with a differential pressure transducer and calculating mass changes at the local temperature and density conditions.

Pipe diameters between 3.2 and 6 mm, and lengths from 30 to 600 mm were used. The release conditions studied represent typical extremes of operation, these being, on the one hand, saturated liquid and long pipes and on the other short pipes down to 30 mm with a level of nitrogen padding to simulate a strongly subcooled entry condition.

RESULTS AND DISCUSSION

An indication of the bubble growth within the flow system is given in figure 5. This shows for three positions down the pipe length, the local diameter and number densities of bubble populations which have arisen from earlier sections of pipe. Identical source populations carry the same symbol, those on the left of the graph corresponding to the positions of first nucleation.

It can be seen that for populations arising from earlier sections, the number density must remain constant, whereas the diameter can grow through the normal bubble growth. The rightmost point in each curve is at the indicated distance. For curve (a) this falls at the end of a cell, while for (b) and (c) it is within a cell. Hence for (b) and (c) the last points are still nucleating, and number and size will increase until the end of the current cell is reached. Also evident is the fact that the smaller diameters are increasing the fastest due to the greater surface/volume ratio.

The principal results of the study are the mass flow rate predictions. These have been evaluated for several sets of data from the literature as well as those of the present study. These data sets are concerned only with straight pipe releases and are detailed in table 1.

Mass flow rates have not been presented, only the percentage errors between the observed and those calculated from the code. These are collected together in figure 6 and further details on these test conditions can be obtained from the references. Diameters range from 52 mm for propane

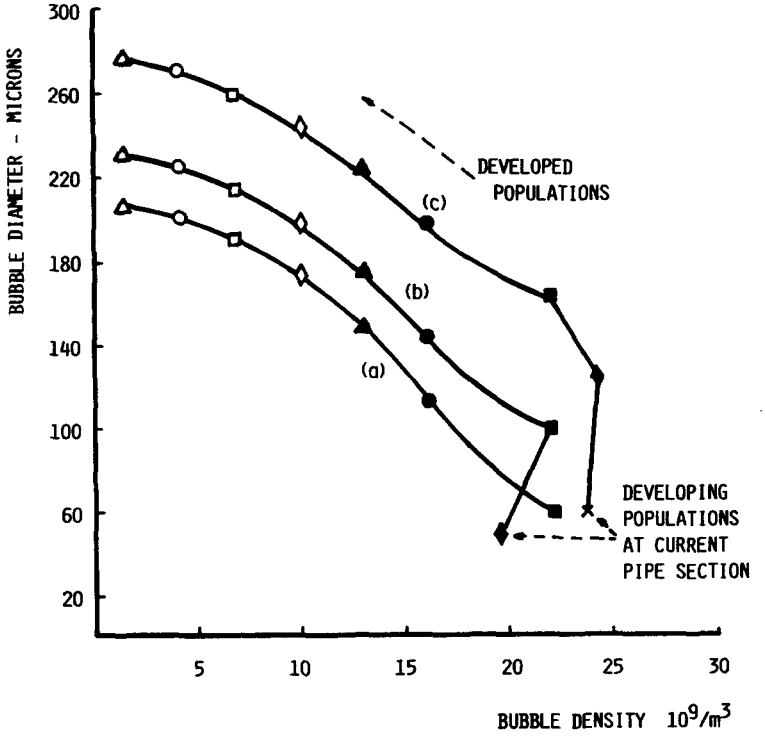

Figure 5. Calculated bubble size distributions at three positions along the release pipe for freon-11. Each symbol corresponds to a particular source cell. Release conditions are $P_0 = 0.4$ MPa, $T_0 = 68°C$, $D = 6$ mm, $L = 300$ mm: (a) distance = 158 mm; (b) distance = 168 mm; (c) distance = 186 mm.

Table 1. Reference data with which code comparison has been made, indicating test numbers, pipe length L (mm), pipe diameter D (mm) and pressure P (MPa)

	No.	L	D	P		No.	L	D	P
	1	40	4	0.73	Fletcher & Johnson (1983)	33	19	3.2	0.40
	2	80	4	0.31	R11	34	35	3.2	0.40
	3	80	4	0.40		35	64	3.2	0.40
	4	80	4	0.49		36	118	3.2	0.40
	5	80	4	0.71		37	160	3.2	0.40
	6	120	4	0.30		38	16	3.2	0.30
	7	120	4	0.40		39	16	3.2	0.37
	8	120	4	0.67		40	16	3.2	0.39
	9	120	4	0.50		41	16	3.2	0.44
	10	60	6	0.28					
	11	60	6	0.40		42	109	15	0.72
Present	12	600	6	0.31	Hurst (1984)	43	55	15	0.67
work	13	300	6	0.31	Propane	44	285	25.8	0.66
R11	14	300	6	0.41		45	55	25.8	0.62
	15	300	3.2	0.31		46	590	52.3	0.68
	16	300	3.2	0.41					
	17	150	3.2	0.33		47	508	12.7	6.46
	18	30	3.2	0.41		48	317	12.7	6.46
	19	50	3.2	0.66	Sozzi & Sutherland (1975)	49	228	12.7	6.46
	20	300	3.2	0.66	Water	50	185	12.7	6.46
	21	640	3.2	0.67		51	106	12.7	6.46
	22	150	4.5	0.67		52	53	12.7	6.46
	23	300	4.5	0.62		53	33	12.7	6.46
	24	300	4.5	0.63		54	12.7	12.7	6.46
	25	450	4.5	0.62					
	26	120	6	0.64		55	254	6.3	9.6
					Fauske (1965)	56	254	6.3	7.6
	27	2000	36	0.42	Water	57	254	6.3	5.5
Nyren &	28	2000	36	0.47		58	254	6.3	1.4
Winters (1983, 1987)	29	3182	32	0.58		59	254	6.3	0.6
SO_2 & NH_3	30	3182	32	0.61					
	31	3182	32	0.59		60	50	4	0.78
	32	3182	32	0.57	Uchida & Nariai (1966)	61	50	4	0.59
					Water	62	20	4	0.78
						63	20	4	0.59
						64	20	4	0.39

releases to 3.2 mm for R11, and L/D ratios from 1 to 200. Errors across this range are generally within a 10% band with a few results giving an error out to 19%.

For the 65 tests calculated, the average error is 7.8%. Of those with larger errors, no particular trend is evident, and it should be noted that no experimental errors have been taken into account. Of interest, however, is the fact that the largest errors of 19% are associated with the short lengths of 16 and 12.7 mm and the errors are positive. There is a bias towards positive errors, as indicated by their algebraic sum which averages to +3%. This, along with larger errors for very short lengths could suggest an underestimate of the heat transfer rate driving evaporation, particularly for the bubble regime. For very long pipes, uncertainty about the wall friction properties can again give

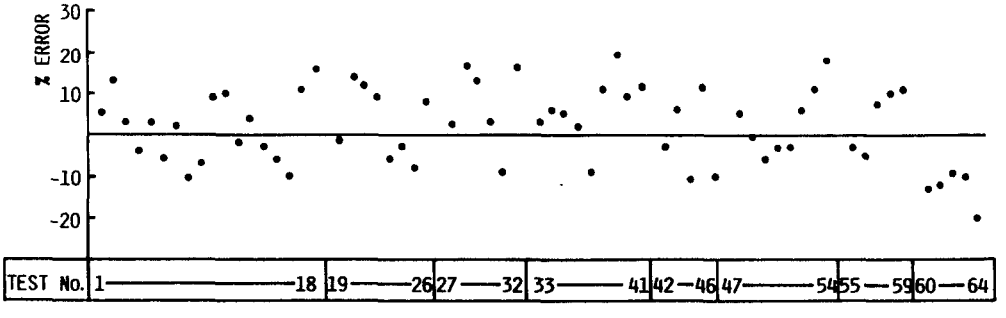

Figure 6. Percentage errors between the observed critical mass flow rates for the test cases indicated in table 1 and those predicted by the modified Richter scheme with wall nucleation.

rise to larger errors since much of the pressure drop arises by this mechanism. In general, however, the solution procedure provides results which are adequate for safety analyses and which indicate the level of errors to be expected in assessing very short releases. In addition, the introduction of a wall nucleation scheme for bubble generation brings this aspect of the code more in line with experimental observations. It is interesting to note that the typical bubble density, obtained by adding the contributions of each population arising from each wall section, is around $8 \times 10^{10}/m^3$, which is close to the optimized value of $10^{11}/m^3$ adopted by Richter (1983).

REFERENCES

ARDRON, K. H. 1978 A two fluid model for critical vapour flow. *Int. J. Multiphase Flow* **4,** 323–337.

BERENSON, P. J. & STONE, R. A. 1965 A photographic study of the mechanism of forced convection vaporisation. *Chem. Engng Prog. Symp. Ser.* **61,** 213–219.

CHURCHILL, S. W. 1977 Friction equation spand all fluid flow regimes. *Chem. Engng* **84,** 91–92.

CLARK, H. B., STRENGE, P. S. & WESTWATER, J. W. 1959 Active sites for nucleate boiling. *Chem. Engng Prog. Symp. Ser.* **55,** 103–110.

EDDINGTON, R. I. & KENNING, D. B. R. 1979 The effect of contact angle on bubble nucleation. *Int. J. Heat Mass Transfer* **22,** 1231–1235.

FAUSKE, H. K. 1965 The discharge of saturated water through tubes. *Chem. Engng Prog. Symp. Ser.* **61,** 211–216.

FLETCHER, B. & JOHNSON, A. E. 1983 The discharge of superheated liquids from pipes. *Ind. chem. Engng Symp. Ser.* **85,** 149–156.

HSU, Y. Y. 1965 Gradual transition of nucleate boiling from discrete bubble regime to multi-bubble regime. *Chem. Engng Prog. Symp.* **61,** 290–298.

HURST, W. J. S. 1984 Combustion of large scale releases of pressurised liquid propane. Presented at the *3rd Symp. on Heavy Gases and Risk Assessment*, Bonn.

LEVY INC. 1982 Critical flow data review and analysis. Report EPRI/NP-2192.

LORENZ, J. J., MIKIC, B. B. & ROHSENOW, W. M. 1975 A gas diffusion technique for determining pool boiling nucleation sites. *Trans. ASME J. Heat Transfer* **May,** 317–319.

MARTINELLI, R. C. & NELSON, D. B. 1948 Prediction of pressure drop during forced circulation boiling of water. *Trans. Am. Soc. mech. Engrs* **70**(6), 695–702.

NYREN, K. & WINTER, S. 1983 Two phase discharge of liquified gases through pipes. Field experiments with NH_3 and theoretical model. Presented at the *4th Int. Symp. on Loss Prevention and Safety Promotion in the Process Industries*, Harrogate.

NYREN, K. & WINTER, S. 1987 Discharge of condensed SO_2: a field test study of the source behaviour with different release geometries. *J. Hazardous Mater.* **14,** 365–386.

RICHTER, H. J. 1983 Separated two phase flow model: applications to critical two phase flow. *Int. J. Multiphase Flow* **9,** 511–530.

SOZZI, G. L. & SUTHERLAND W. A. 1975 Critical flow of saturated and subcooled water at high pressure. Presented at the *ASME Symp. on Non-equilibrium Two Phase Flow*, Houston, Tex.

UCHIDA, H. & NARIAI, H. 1966 Discharge of saturated water through pipes and orifices. In *Proc. 3rd Int. Heat Transfer Conf.*, Vol. 5, p. 1, Chicago, Ill.

YILMAZ, S. & WESTWATER, J. W. 1980 Effect of velocity on heat transfer to boiling freon 113. *Trans. ASME J. Heat Transfer* **102,** 26–31.